

3-D rare earth-doped colloidal photonic crystals

M. Clara Gonçalves^a, Luis M. Fortes^a, Rui M. Almeida^{a,*}, Alessandro Chiasera^b,
Andrea Chiappini^b, Maurizio Ferrari^b

^aDepartamento de Engenharia de Materiais/ICEMS, Instituto Superior Técnico/TU Lisbon, Av. Rovisco Pais, 1049-001 Lisboa, Portugal

^bIFN-CNR, Istituto di Fotonica e Nanotecnologie, CSMFO group, 38050 Povo – Trento, Italy

ARTICLE INFO

Article history:

Available online 28 November 2008

PACS:

42.70.Qs

64.70.pv

81.20.Fw

78.55.Qr

Keywords:

Colloidal photonic crystals

3-Dimensional photonic crystals

Sol-gel

Opals

Inverse opals

Er doping

ABSTRACT

Three-dimensional photonic bandgap structures have been synthesized by a colloidal/sol-gel route, starting with the self-organization of polystyrene microspheres into opal structures by vertical convective self-assembly, followed by sol-gel infiltration of the interstices with silica or titania doped with Er^{3+} and Yb^{3+} ions and the removal of the polymeric template by heat treatment. The structural and optical properties of the opals and inverse opals prepared by this method have been studied by scanning electron microscopy and near infra-red spectroscopy. The SEM images show that the photonic crystals contain ordered domains up to $\sim 600 \mu\text{m}^2$. Variable incidence reflectivity spectra have been measured for the opals, infiltrated opals and inverse opals. The corresponding effective refractive indices (n_{eff}) were calculated based on effective-medium approaches. Photoluminescence measurements of the emission of Er^{3+} ions at $\sim 1.5 \mu\text{m}$ from titania inverse opal structures were performed and are compared with those characteristic of the same ions in bulk titania material in the absence of a photonic bandgap structure.

© 2008 Elsevier B.V. All rights reserved.

1. Introduction

In recent years, photonic crystals (PCs) have been attracting much interest due to their unique properties, such as the existence of photonic bandgaps (PBGs), the appearance of localized states of light when a defect is introduced in the otherwise regular lattice and the suppression or enhancement of non-linear effects. PCs are artificial composite materials characterized by a periodicity in the dielectric constant, where light within a certain frequency range cannot propagate. If the PC is periodic on a scale of a few hundreds of nm, then a certain range of frequencies in the visible or near infra-red range will be completely reflected, due to the Bragg reflection [1] rather than the Fresnel reflection. The forbidden frequency range is called a stop band [2,3]. Great effort has been directed towards the development of materials with complete photonic band gaps, particularly in the visible range [4–6].

Traditionally, two approaches have been used to fabricate photonic crystals: nanolithography (the *top-down approach*) [7,8] and self-assembly of colloidal spheres (a *bottom-up approach*) [9–12]. Colloidal PCs, also known as artificial opals, seem the most likely candidates for 3-D PCs. Self-assembly techniques have many potential advantages in opal fabrication, offering significantly lower

costs and being more compatible with very large scale integration technologies than conventional lithographic techniques. The main disadvantage, common to all the methods involved in opal and inverse opal fabrication up to now, is the presence of a relatively large number of structural defects, which are inherent to the synthesis mechanism of the opals and can be copied to the inverse structures, largely restricting their possible applications.

The photoluminescence (PL) of Er^{3+} ions at $\sim 1.5 \mu\text{m}$ is very important for laser action and for amplification in the third window of present day telecommunications and rare-earth PL inside PC's may exhibit interesting unusual characteristics [13]. In addition, Yb^{3+} ions have a much larger absorption cross-section near 975 nm than Er^{3+} ions, such that Yb^{3+} can act as a sensitizer for the Er^{3+} emission near $\sim 1.5 \mu\text{m}$, through Forster energy transfer. Such energy transfer phenomena may be enhanced in PC structures [13,14]. The present work includes PL results in $\text{Er}^{3+}/\text{Yb}^{3+}$ doped inverse opals which show enhancement of Er^{3+} emission from the PCs and $\text{Yb}^{3+} \rightarrow \text{Er}^{3+}$ energy transfer within the PC structures.

2. Experimental

2.1. Fabrication of opal structures

Monodisperse polystyrene (PS) spheres with a nominal diameter (D) of 460 nm, as a 10 wt% dispersion in water, were purchased

* Corresponding author. Tel.: +351 218418110; fax: +351 218418132.

E-mail address: rui.almeida@ist.utl.pt (R.M. Almeida).

from Aldrich. Upon dilution, 0.1 wt% PS suspensions were prepared in deionised water and dispersed by sonication for 20 min. Microscope slides cut in half ($7.5 \text{ cm} \times 1 \text{ cm}$) were used as substrates. Vertical convective self-assembly deposition was achieved with each substrate placed vertically in a vial containing the colloidal suspension, in an oven at $50 \text{ }^\circ\text{C}$. The colloidal crystal was then dried for 10 min at $50 \text{ }^\circ\text{C}$. The final product was a compact of spheres with several tens of planes. Further details can be found in Ref. [12].

2.2. Fabrication of inverse opal structures

The PS colloidal crystals were used as templates for fabricating silica and titania inverse opal structures. The SiO_2 and TiO_2 sols were prepared by sol-gel processing; in the case of doped titania infiltrated and inverse opals, the dopant concentrations added to the TiO_2 sol were between 0.25% and 1% Er^{3+} and 1–2.5% Yb^{3+} . Further details can be found in Ref. [12]. The voids in the self-assembled PS opal templates were infiltrated with silica or titania precursors via sol-gel dip-coating. The substrate covered by the template was lowered into the precursor solution and then withdrawn at a low speed ($\sim 2 \text{ cm min}^{-1}$), while the silica or titania sols penetrated the voids of the PS colloidal crystal by capillary forces. Finally, the PS template was removed by heat treatment as the samples were slowly heated to $450 \text{ }^\circ\text{C}$ ($@ 0.5 \text{ }^\circ\text{C min}^{-1}$) and left at this temperature for 30 min; some were further heated to $900 \text{ }^\circ\text{C}$ and left at this temperature for 15 min. The PS spheres decomposed, leaving air spheres in a dielectric matrix inverse opal.

2.3. Characterization

A Hitachi S-2400 scanning electron microscope (SEM) was used to study the structures of the PCs prepared, in the secondary electron mode. Optical transmission and reflection spectra in the visi-

ble and infra-red regions were measured at room temperature, with a Fourier Transform infrared (FTIR) Thermo Nicolet 5700 spectrometer, equipped with a quartz beamsplitter, a DTGS detector and a white light source, at a resolution of 4 cm^{-1} .

Unpolarized Raman spectra excited with the 514.5 nm line of a Spectra-Physics 2016 Argon ion laser, were collected with a Spex 1403 double monochromator and detected with a photomultiplier tube.

PL spectroscopy in the region of the ${}^4\text{I}_{13/2} \rightarrow {}^4\text{I}_{15/2}$ transition of Er^{3+} was excited with the 514.5 nm line of an Argon ion laser, or the 980 nm emission from a titanium:sapphire laser. The luminescence was dispersed by a 320 mm single-grating monochromator, with a resolution adjusted in each case. The light was detected with a NIR photomultiplier tube and standard lock-in technique.

3. Results and discussion

3.1. SEM characterization of opal and inverse opal structures

The opals, sol-gel infiltrated opals and inverse opals exhibited iridescence, easily observed with the naked eye, due to scattering and Bragg light reflection.

Fig. 1a shows a typical SEM image of a PS opal obtained by convective self-assembly synthesis, which exhibits *fcc* structure with the $[111]$ direction normal to the sample surface. The infiltration of the sol-gel precursor did not significantly alter the *fcc* arrangement of the PS opal template, although some PS sphere shrinkage did occur (linear contraction of $\sim 10\%$ from initial sphere diameter) due to the mild heat treatment at this stage (10 min at $50 \text{ }^\circ\text{C}$). The silica inverse opal structure was found to replicate the PS opal template, with a linear contraction of $\sim 20\%$ in the diameter of the voids created by the PS sphere heat removal (Fig. 1b and c). Similar results were obtained for titania inverse opals.

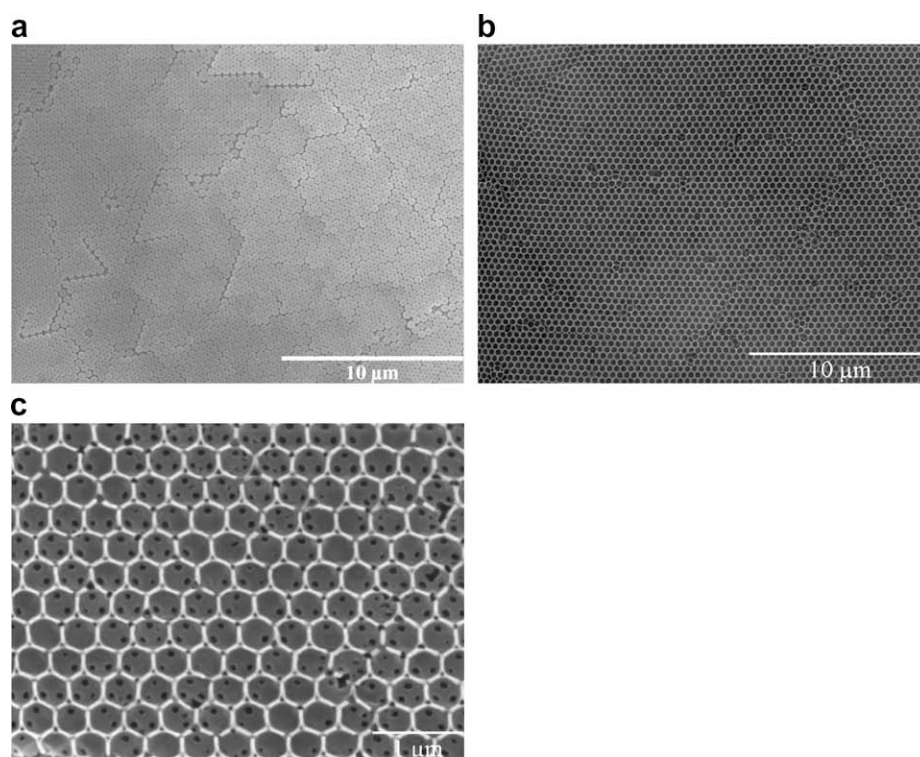


Fig. 1. SEM micrographs of 460 nm PS sphere-derived PCs made by convective self-assembly from a $0.1 \text{ wt}\%$ suspension in water: (a) PS opal; (b) and (c) silica inverse opal, consisting of air spheres in a silica matrix.

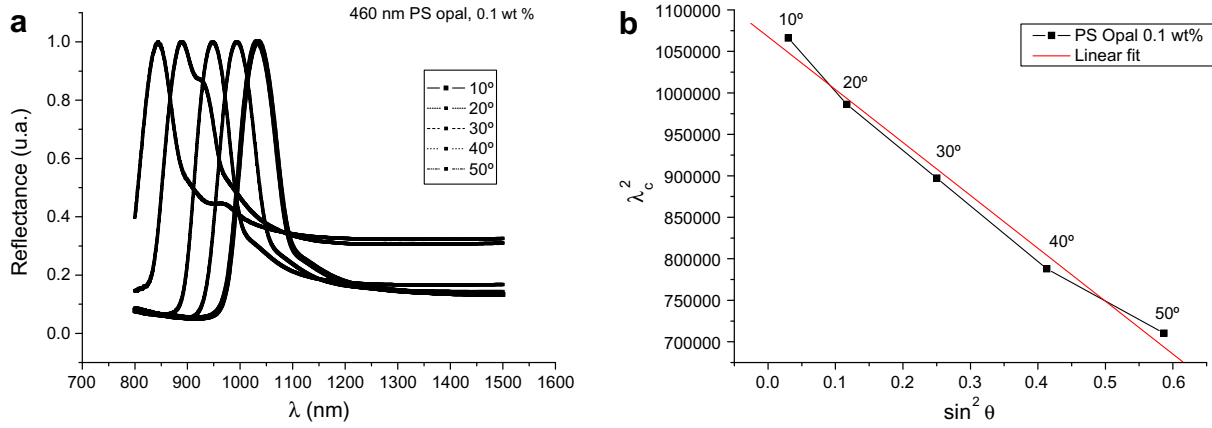


Fig. 2. (a) Normalized optical reflectivity at different angles of incidence of an opal structure made by convective self-assembly of a 0.1 wt% suspension of 460 nm PS spheres in water (the incidence angle increased from 10° to 50°, in steps of 10°, from right to left); (b) plot of λ_c^2 vs. $\sin^2\theta$.

Table 1
Comparison between measured and calculated effective refractive indices of photonic crystals.

	$\epsilon_{\text{eff}} = \epsilon_1 \left(\frac{2\epsilon_1 + \epsilon_2 + 2f(\epsilon_2 - \epsilon_1)}{2\epsilon_1 + \epsilon_2 - f(\epsilon_2 - \epsilon_1)} \right)$		$(n_{\text{eff}}^2 - 1)/(n_{\text{eff}}^2 + 2) = (1-f)(n_2^2 - 1)/(n_2^2 + 2) + f(n_1^2 - 1)/(n_1^2 + 2)$	$n_{\text{eff}} = fn_1 + (1-f)n_2$	$n_{\text{eff}}^2 = fn_1^2 + (1-f)n_2^2$
	$n_{\text{eff}}^{\text{meas}}$	$n_{\text{eff}}^{\text{calc}}$			
PS opal	1.33	1.19	1.41	1.44	1.46
PS opal + TiO ₂ (infiltrated)	1.36	1.31	1.68	1.70	1.71
PS opal + SiO ₂ (infiltrated)	1.51	1.24	1.55	1.55	1.56
TiO ₂ – inverse opal	1.10	1.11	1.20	1.26	1.33
SiO ₂ – inverse opal	1.01	1.05	1.11	1.12	1.13

3.2. Photonic properties of opal structures

Fig. 2a shows experimental angle resolved reflectance spectra of a PS opal, with sphere diameters of 460 nm. The height of the reflectivity peaks (the measured reflectance reached up to ~50% relatively to an aluminum mirror background) depends on the thickness and the quality of the opal crystal.

For near-normal incidence (10° off-normal), the [111] Bragg reflection peaks were observed near 1032 nm for the PS opal (Fig. 2a). The centre frequency of the stop band (λ_c) depends on the interplanar spacing between the scattering planes, d , on the filling fraction of the high index material, f and on the magnitude of the refractive index contrast between the materials which form the PC structure. The PS stop band positions (λ_c) show a clear blue shift with increasing off-normal incidence angle, expressed by a modification of Bragg’s law which takes into account Snell’s law of refraction, valid in the optical regime [15]:

$$\lambda_c = 2d\sqrt{n_{\text{eff}}^2 - \sin^2\theta}, \quad (1)$$

where θ is the angle between the incident radiation and the normal to the set of planes and n_{eff} is the effective refractive index of the PC composite. Experimentally, d and n_{eff} may be determined by measuring the position of the reflectance maximum at different angles of incidence and plotting λ_c^2 versus $\sin^2\theta$, as shown in Fig. 2b for the PS opal. If the Bragg diffraction conditions are satisfied, a straight line will result with a slope $-(2d)^2$ and y-axis intercept $(2d n_{\text{eff}})^2$. Since the Bragg reflections occur from the (111) planes (parallel to the substrate), which are the most densely packed in the fcc arrangement, the interplanar spacing $d_{hkl} = \frac{a}{\sqrt{h^2+k^2+l^2}}$ yields $d_{(111)} = \frac{a}{\sqrt{3}}$, where $a = \frac{2D}{\sqrt{2}}$ and thus $D = \sqrt{\frac{3}{2}}d$, D being the sphere diameter of the colloidal PC. From the slopes of the above plots, a D value of 470 nm was obtained for the PS opal, in excellent agreement with the nominal value ($D = 470$ nm).

The intercepts yielded $n_{\text{eff}}^{\text{meas}}$ values of 1.33 and 1.17, for the PS and silica opals, respectively. Table 1 lists, for several examples

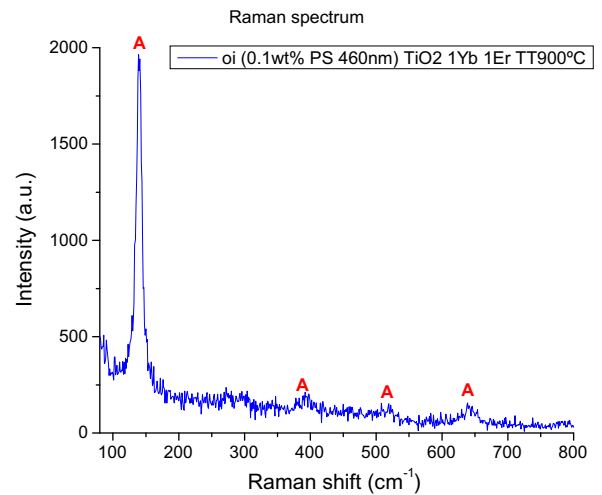


Fig. 3. Raman spectrum of titania inverse opal, heat treated at 900 °C for 15 min.

of opal, infiltrated opal and inverse opal crystals, a comparison of the measured effective refractive index (n_{eff}) with those calculated ($n_{\text{eff}}^{\text{calc}}$) based on different effective-medium approaches. The Maxwell–Garnett and the Lorentz–Lorenz approximations, both based on the Clausius–Mossotti equation, are the most widely used for calculating the bulk dielectric properties of inhomogeneous materials, but other expressions have been proposed for the effective permittivity ($\epsilon_{\text{eff}} = n_{\text{eff}}^2$) of a composite medium [16]. The simplest ones are the mixing rules, based on n or ϵ additivity, for example:

$$\epsilon_{\text{eff}} = f\epsilon_1 + (1-f)\epsilon_2, \quad (2)$$

where f takes the value 0.74 for fcc packing, as in the case of PS opal; ϵ_1 represents the PS or the silica relative dielectric constant ($\epsilon_{\text{PS},d} = 2.53$; $\epsilon_{\text{SiO}_2,d} = 2.10$) and ϵ_2 the air dielectric constant ($\epsilon_{\text{air},d} = 1$), where d refers to the helium yellow line at 587.6 nm. Discrepancies

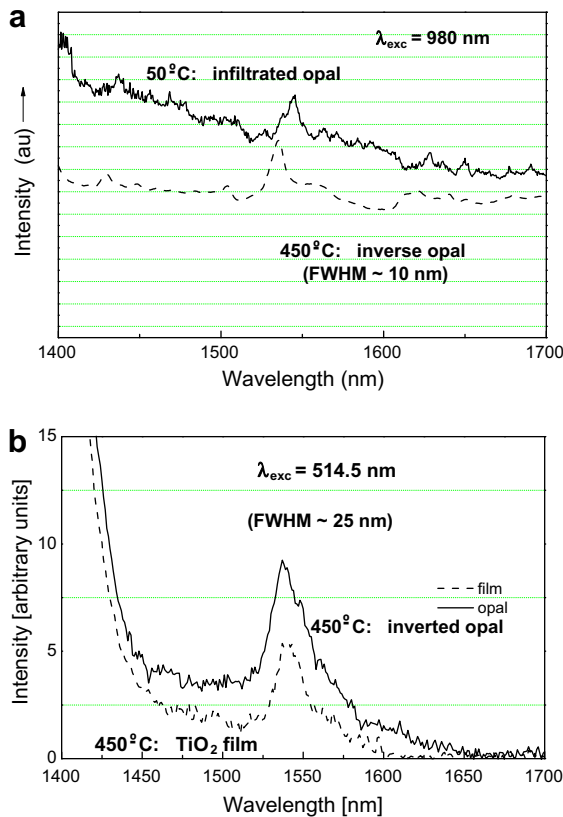


Fig. 4. Room temperature Er^{3+} PL spectra of PC structures doped with 0.75% Er and 2.5% Yb: (a) titania infiltrated PS opal vs. titania inverse opal; (b) titania inverse opal vs. doped titania film.

between the measured and calculated n_{eff} values are not surprising, due to disorder in the PCs and also to the fact that the effective-medium approach is expected to hold only when the PC lattice parameter ($\sim 0.5 \mu\text{m}$) is well below the wavelength of light ($\sim 1 \mu\text{m}$), which is not the case.

3.3. Photonic properties of inverse opal structures

The reflection spectra of silica and titania inverse opal structures have been measured, but are not shown here due to space limitations. The [111] Bragg reflection can be observed near 870 and 940 nm, respectively, for near-normal incidence condition (10° off-normal). From the slopes of the plots of λ_c^2 vs. $\sin^2\theta$, n_{eff} values of 1.01 and 1.10 were obtained for silica and titania inverse opals, respectively, in reasonable agreement with calculated values (Table 1).

3.4. Raman and PL spectra of $\text{Er}^{3+}/\text{Yb}^{3+}$ -doped inverse opal structures

Fig. 3 shows a typical unpolarized Raman spectrum of a titania inverse opal heat treated at 900°C . All the peaks marked with A are characteristic of the anatase phase of TiO_2 .

Fig. 4a shows the $^4\text{I}_{13/2} \rightarrow ^4\text{I}_{15/2}$ PL spectra of Er/Yb-doped titania infiltrated and inverse opal structures, upon excitation at 980 nm. No Er^{3+} PL was observed from the infiltrated opal, probably due to quenching from residual OH groups not removed at 50°C . The PL from the inverse opal had a narrow bandwidth ($\sim 10 \text{ nm}$), but titania was still amorphous after heated at 450°C , as verified by Raman spectroscopy. The spectra excited at 514.5 nm were much weaker (thus noisier) and required a broader slit width, thus the larger bandwidth of $\sim 25 \text{ nm}$ (Fig. 4b). This fact indicates that the signal at 980 nm was stronger, probably due to $\text{Yb}^{3+} \rightarrow \text{Er}^{3+}$ energy transfer. The film had a weaker PL signal than the titania photonic crystal; this could be due to PL enhancement in the PC, but further confirmation will be needed.

4. Conclusions

Sol-gel processing is a simple, inexpensive method for the preparation of PCs such as (1-D) Bragg mirrors and microcavities or (3-D) synthetic opals and inverse opals, with possible application in a range of optical components and devices. Good quality 3-D photonic crystals can easily be prepared by colloidal/sol-gel processing (vertical convective self-assembly of monodisperse dielectric spheres) in the form of opals, infiltrated opals and inverse opals with well ordered regions up to $\sim 600 \mu\text{m}^2$. Inverse opal structures can be doped with rare-earth ions like Er^{3+} and Yb^{3+} , whose PL may be enhanced due to $\text{Yb}^{3+} \rightarrow \text{Er}^{3+}$ energy transfer and also likely to an increased interaction of light within a PC structure.

References

- [1] J.D. Joannopoulos, R.D. Meade, J.N. Winn, Photonic Crystals: Molding the Flow of Light, Princeton University Press, 1995. Chapter 3.
- [2] E. Yablonovitch, Phys. Rev. Lett. 58 (1987) 2059.
- [3] S. John, Phys. Rev. Lett. 58 (1987) 2486.
- [4] S.Y. Lin, J.G. Fleming, D.L. Hetherington, B.K. Smith, R. Biswas, K.-M. Ho, M.M. Sigalas, W. Zubrzycki, S.R. Kurtz, J. Bur, Nature 394 (1998) 251.
- [5] A. Blanco, E. Chomski, S. Grabtchak, M. Ibisate, S. John, S.W. Leonard, C. Lopez, F. Meseguer, H. Miguez, J.P. Mondla, G.A. Ozin, O. Toader, H.M. van Driel, Nature 405 (2000) 427.
- [6] V.L. Colvin, MRS Bull. 26 (2001) 637.
- [7] S. Noda, K. Tomoda, N. Yamamoto, A. Chutinan, Science 289 (2000) 604.
- [8] M. Qi, E. Lidorikis, P.T. Rakich, S.G. Johnson, J.D. Joannopoulos, E.P. Ippen, H.I. Smith, Nature 429 (2004) 538.
- [9] R.M. Almeida, S. Portal, Curr. Opin. Sol. State Mater. Sci. 7 (151–157) (2003) 151.
- [10] R.M. Almeida, M.C. Gonçalves, S. Portal, J. Non-Cryst. Solids 345&346 (2004) 562–569.
- [11] R.M. Almeida, M.C. Gonçalves, Sol-gel derived photonic bandgap structures, in: R. Balda (Ed.), Photonic Glasses, Research Signpost, Kerala, India, 2006, pp. 67.
- [12] M.C. Gonçalves, J. Brás, R.M. Almeida, J. Sol-Gel Sci. Techno. 42 (2007) 135.
- [13] R.M. Almeida, A.C. Marques, A. Chiasera, A. Chiappini, M. Ferrari, J. Non-Cryst. Solids 353 (2007) 490–493.
- [14] R.M. Almeida, A.C. Marques, S. Portal, Opt. Mat. 27 (2005) 1718–1725.
- [15] C. Lopez, L. Vazquez, F. Meseguer, R. Mayoral, M. Ocana, H. Miguez, Superlattices Microstruct. 22 (1997) 399.
- [16] S. Datta, C.T. Chan, K.M. Ho, C.M. Soukoulis, Phys. Rev. B 48 (1993) 14936.